

## Article

# Multi–Objective Collaborative Optimization Design of Key Structural Parameters for Coal Breaking and Punching Nozzle

Lihuan Chen <sup>1,2</sup>, Muzheng Cheng <sup>2</sup>, Yi Cai <sup>2</sup>, Liwen Guo <sup>3</sup> and Dianrong Gao <sup>1,\*</sup><sup>1</sup> School of Mechanical Engineering, Yanshan University, Qinhuangdao 066004, China; chenlihuan522@163.com<sup>2</sup> School of Mechanical and Electrical Engineering, North China Institute of Aerospace Engineering, Langfang 065000, China; cmuzheng@sina.com (M.C.); caiyi720906@sina.com (Y.C.)<sup>3</sup> College of Mining Engineering, North China University of Science and Technology, Tangshan 063210, China; guoliwen@ncst.edu.cn

\* Correspondence: gaodr@ysu.edu.cn

**Abstract:** The technology of coal breaking and punching by a high-pressure water jet can increase the permeability of coal seam and prevent gas explosion accidents. As one of the key components of this technology, the structural parameters of the nozzle have an important effect on the performance of the water jet. At present, the relationship between multiple optimization indexes and structural parameters of the nozzle is mostly studied separately. In fact, the influence of the nozzle structural parameters on different optimization indexes is different. When there are multiple optimization indexes, they should be considered collaboratively to achieve the best water jet performance of the nozzle. Therefore, a multi–objective collaborative optimization method is proposed which takes the maximum velocity in X-axis and effective extension distance in Y-axis as the performance evaluation indexes of the water jet. The numerical simulation of the nozzle jet is carried out by computational fluid dynamics(CFD) method, and an orthogonal test database is established. The weight of multi-objective is analyzed, and the key structural parameters of the nozzle are optimized by the combination of BP (back propagation) neural network and genetic algorithms. The results show that the primary and secondary sequence of each structural parameter on is  $\gamma > \theta > l/d$ , which could reflect the comprehensive influence on the maximum velocity in the X-axis and effective extension distance in the Y-axis. The optimal structural parameters of the nozzle are,  $\theta = 42.512^\circ$ ,  $l/d = 2.5608$ ,  $\gamma = 12.431^\circ$ . The field erosion experiment shows that compared with the original nozzle, the water jet performance of the optimized nozzle has been improved, the punching depth has been increased by 72.71%, and the punching diameter has been increased by 106.72%. This study provides a certain reference for the design and optimization of coal breaking and punching nozzle.

**Keywords:** nozzle; water jet; orthogonal test; multi-objective collaborative optimization; BP neural network; genetic algorithm



**Citation:** Chen, L.; Cheng, M.; Cai, Y.; Guo, L.; Gao, D. Multi–Objective Collaborative Optimization Design of Key Structural Parameters for Coal Breaking and Punching Nozzle. *Processes* **2022**, *10*, 1036. <https://doi.org/10.3390/pr10051036>

Academic Editors: Yong Zhu, Qiang Gao, Xiaoming Yuan, Chuan Wang and Bo Hu

Received: 11 May 2022

Accepted: 20 May 2022

Published: 23 May 2022

**Publisher’s Note:** MDPI stays neutral with regard to jurisdictional claims in published maps and institutional affiliations.



**Copyright:** © 2022 by the authors. Licensee MDPI, Basel, Switzerland. This article is an open access article distributed under the terms and conditions of the Creative Commons Attribution (CC BY) license (<https://creativecommons.org/licenses/by/4.0/>).

## 1. Introduction

In recent years, with the development of fluid control technology, especially with the synergy of modern advanced decision-making and control methods such as fuzzy logic, machine learning, or artificial intelligence, the application of the water jet technology should be more and more extensive, especially in the fields of coal, petroleum, metallurgy, etc. [1–3]. Since a water jet has the advantage of high efficiency, being dust-free and maintain a low heat in the process of crushing coal and rock medium, and meeting harsh environmental conditions, it has been widely used in “pressure relief antireflective” technology in recent years, such as hydraulic punching, hydraulic slotting, and hydraulic cutting and so on [4,5]. The research shows that the stress distribution of surrounding coal can be changed during coal breaking and punching by the water jet, which can promote the expansion and development of coal rock fissures, release the elastic energy in coal and rock, increase the

permeability of coal seam, and then raise gas drainage amount and reduce coal mining accidents [6–9]. As one of the important components of the water jet equipment, the nozzle converts the static pressure of the water into water power, and its structure directly affects the flow and dynamic characteristics of the water jet [10–13]. Therefore, it is of great significance to study the relationship between the key structure of the nozzle and the performance of the water jet and optimize the key parameters of the nozzle to improve the performance of the water jet.

Wen et al. [14] designed a bionic straight cone nozzle with circular groove-type bionic units inside. Through the design and implementation of the orthogonal experiment, the influence of structural parameters of the bionic straight cone nozzle on impact force index is explored, and the bionic nozzle structure is optimized to obtain the best structural parameters. Then, through CFD simulation and experimental analysis, it is found that the performance of bionic straight cone nozzle is better than that of ordinary straight cone nozzle for three reasons: the liquid buffer effect, the auxiliary thrust effect, and the liquid rolling bearing effect. On the basis of fully considering the energy loss and nozzle parameters, Yang et al. [15] established the water jet reaction force model, obtained the relationship between nozzle shape and energy loss, and optimized the nozzle. The reaction force and energy conversion rate of the optimized nozzle have been significantly improved, which has guiding significance for the improvement of the water jet propulsion system. Zhang et al. [16] designed the divergent surface of a supersonic minimum length nozzle (MLN) specially for laser-assisted oxygen cutting (LASOX) based on the method of characteristic quantities (MOC). Through numerical simulation and experimental verification, the nozzle significantly improved the cutting quality. Chen et al. [17] explored the influence of the key structural parameters of the nozzle on the water jet performance, and optimized the nozzle structure to improve the jet performance by considering the interaction between the structural parameters. Juraeva et al. [18] and others took the water resistance of textile nozzle as the optimization objective function, established the optimization database of taper, slotting and jet ring length by using Minitab software, and obtained the optimal nozzle parameter combination, which effectively improved the water resistance. Onuret al. [19] established the linear regression model between the key parameters of the printing nozzle and the print quality based on the experimental data, studied the influence of the key parameters on the print quality, and optimized the nozzle channel. The optimized nozzle has been experimentally verified to be effective in improving the accuracy of printed parts. Wang et al. [20] studied the influence of the nozzle structure parameters on the descaling effect of coal mine pipeline, and obtained the best nozzle structure parameters under different pressure and flow conditions by using the method of orthogonal test, which has certain guiding significance for water jet descaling. In terms of multi-parameter models, Tang et al. [21–24] proposed an improved convolution neural network (CNN) method to train the multi-parameter model of piston pump, and then used a Bayesian Optimization (BO) method to select the optimal combination, the experiment shows that the improved CNN-BO method has high accuracy in fault diagnosis. Ding et al. [25] took the total pressure coefficient and efficiency of low-pressure axial flow fan as the optimization objectives, and used NSGA-II algorithm to optimize its structural parameters, which provided a reference for the multi-objective optimization problem. Cain et al. [26] built a prediction model of foreign exchange rate based on artificial neural networks (ANN) and genetic algorithms (GA), its prediction accuracy can reach 72.5% and has high generalization, which fully shows the advantages of ANN-GA algorithm in building the model. Abbas et al. [27] established a mathematical model for the generation of entropy in magneto hydrodynamic radiative reactive, optimized multiple parameters by using the combination of artificial neural network (ANN) and particle swarm optimization algorithm (PSO), and finally obtained the minimum entropy, showing the powerful optimization capability of ANN-PSO algorithm for multi-parameter complex models.

From the above research and analysis, it can be seen that at present, the research on nozzle optimization at home and abroad mainly focuses on single evaluation index and

single optimization method, while there is less research on the interaction between multiple parameters and multi-objective optimization in the overall structure. However, the multi-parameter and multi-objective analysis of coal breaking and punching nozzle plays a key role in improving water jet performance and solving the problems in practical application. Therefore, based on the operability of the nozzle processing and field experience, the key parameters of coal breaking and punching nozzle are optimized by the method combining numerical simulation and intelligent collaborative optimization in this paper. This study reveals the influence rule of key structural parameters on the maximum velocity in X-axis and effective extension distance in Y-axis, determines the optimal structural parameters of the nozzle. It is verified experimentally that the nozzle with the optimal combination of structural parameters effectively improves the coal breaking and punching ability of the water jet, which provides a technical reference for the multi-parameter and multi-objective optimization of the nozzle.

## 2. Numerical Simulation and Analysis

### 2.1. Structure and Key Parameters of the Nozzle

Due to the small inner diameter of the nozzle, in order to facilitate processing, the split design is adopted. The nozzle is divided into contraction section and outlet section. The two parts are connected by metal sealing ring and nozzle sleeve. The specific structure is shown in Figure 1. The inlet pressure is 15–20 MPa, and it is injected with a higher speed through the acceleration of the contraction section and the steady flow of the exit section.

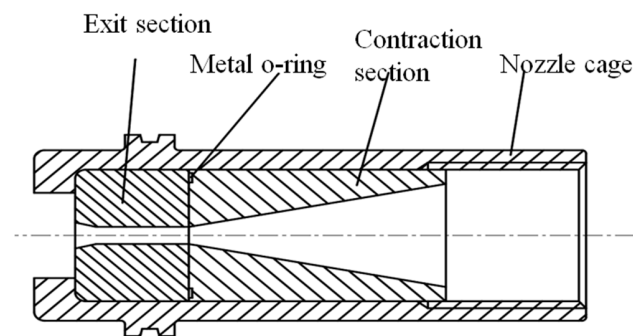


Figure 1. Structure of the nozzle.

The research shows that [28–34], the key factors affecting the performance of the water jet are contraction angle, length-to-diameter ratio (the ratio of outlet cylinder length  $L$  to cylinder diameter  $d$ ) and outlet expansion angle, and the change of their parameters directly affects the water jet performance. Therefore, these three parameters are also the focus of research and optimization in this paper, and the schematic diagram of the structural parameters is shown in Figure 2.  $l$  is the length of the outlet cylinder section, its length is determined by the length-to-diameter ratio.  $l'$  is the length of the outlet divergence angle, in this paper  $l' = 1$  mm.  $L$  is the length of the contraction section and the calculation equation is as follows:

$$L = \frac{D}{2} \cot \frac{\theta}{2} - \frac{d}{2} \cot \frac{\theta}{2} \quad (1)$$

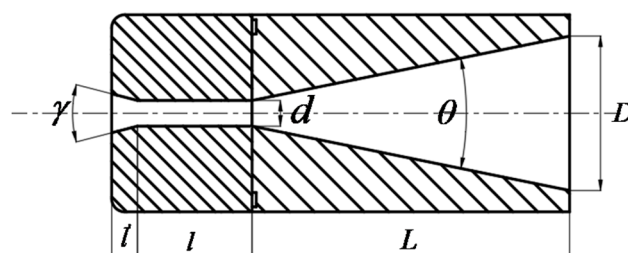


Figure 2. Diagram of the nozzle structure.

## 2.2. Numerical Simulation and Boundary Condition

In the high-pressure water jet impact process under non-submerged conditions, there will be violent turbulent diffusion and momentum exchange between the water and the air in the surrounding environment, which belongs to the multi-phase flow problem. Therefore, computational fluid dynamics (CFD) method is used to simulate the process of the water jet. In order to avoid the influence of the flow field boundary on the calculation results, the external flow field area should be large enough, according to this paper, the external flow field is set to a 60 mm × 60 mm × 200 mm rectangular body.

When the high-pressure water is accelerated by the nozzle, it will be injected into the air with a very high velocity, and the water jet will continuously suck in the air at the boundary, at the same time, the water droplets are “torn” by aerodynamic forces, which produces a velocity difference between the two. Therefore, the numerical simulation is carried out using the Mixture model of the multiphase flow model, with the main phase set to air and the second phase set to water. The transient and implicit pressure solver are used for calculation, the turbulence model is two-equation model of RNG K- $\epsilon$ . The conical end face of the nozzle is set to ‘Pressure-inlet’, the pressure is set to 20 MPa, the inner surface of the nozzle is set to ‘Wall’, the external flow field area is set to Pressure-outlet, and the pressure is set to one atmosphere. The SIMPLE pressure-velocity coupling algorithm is used to solve the control equations [35,36].

## 2.3. Model Meshing and Independence Verification

In order to ensure the accuracy of numerical simulation and improve the simulation efficiency of computer, the computational model is divided by the hybrid grid technology. Inside and outlet of the nozzle, the structure size is small, local pressure is large, and turbulence is intense. Hence, an unstructured grid is used to divide the nozzle, as shown in Figure 3. The external flow field of the nozzle is large and regular in shape, the rebythe structured regular hexahedron grid is used to divide it, which can reduce the number of grids and improve the calculation efficiency. In addition, in order to accurately simulate the entrainment effect of the water jet on the surrounding air, the external flow field area is divided by the density gradient meshing method, and the grid in the area with complex flow is encrypted, as shown in Figure 4.

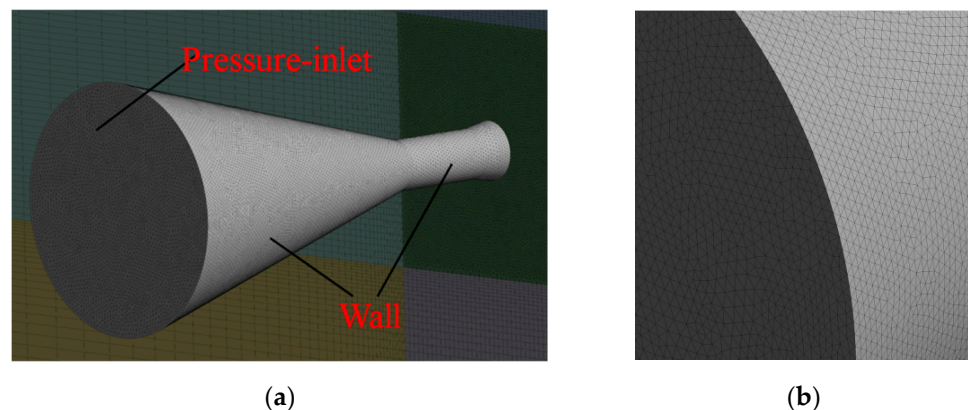


**Figure 3.** Simulation Model of the nozzle: (a) unstructured grid of the nozzle; (b) detail view of unstructured grid.

The number of computational grids affects the accuracy and efficiency of numerical calculation. Too few grids will affect the accuracy of results. However, if the number of grids continues to increase after reaching a certain number, it will not only improve the computational accuracy, but also reduce the computational efficiency. Therefore, it is necessary to verify the independence of the grid number in the computational domain to determine the optimal grid number. Firstly, a group of grids are determined as the benchmark, in which the grid number of the nozzle is 1,257,283 and the grid number of

flow field is 4,987,351. Secondly, the independence of the grid is verified based on the above boundary conditions. Taking the maximum velocity in X-axis at 100 mm away from the nozzle outlet as the standard, the deviation of this value between each grid number and the reference grid is calculated, the results are shown in Table 1, where the deviation 0 represents the benchmark grid. It can be seen from the results that all deviations are within 0.3%. The nozzle and flow field are re-divided and calculated according to the minimum number of grids in Table 1. Compared with the reference grid results, the deviation is 0.29%, which meets the grid-independent requirement, the selected number of reference grids can be calculated later.

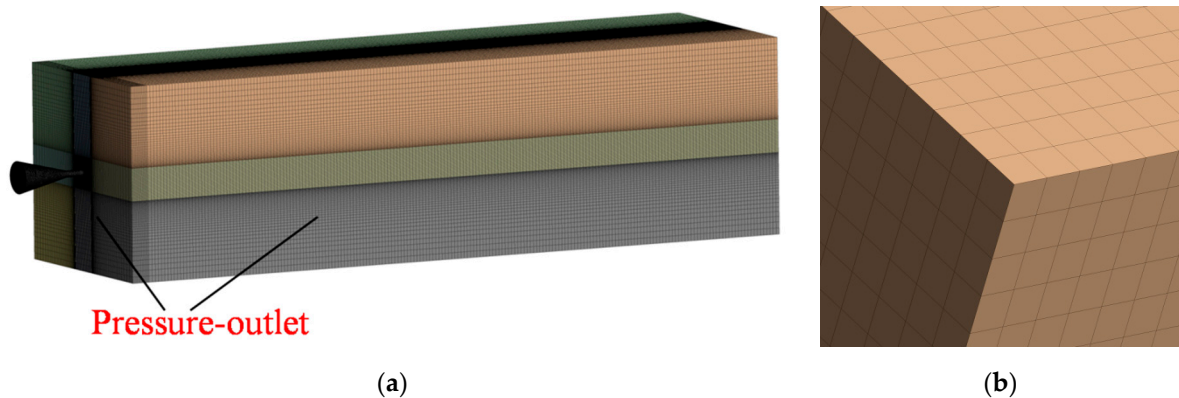


**Figure 4.** Simulation Model of Flow Field: (a) structured grid of flow field; (b) detail view of structured grid.

**Table 1.** Verification of grid independence.

Area	Number of Grid	Maximum Velocity of X-axis (m/s)	Deviation (%)
Nozzle	643,765	199.241	0.212
	1,257,283	199.865	0
	2,345,759	199.395	0.115
Externalflowfield	4,165,783	199.383	0.241
	4,987,351	199.865	0
	5,634,524	200.068	0.102

The research shows that when continuous water jet impinges vertically on the surface of an object, it actually converts the kinetic energy of the water jet into dynamic pressure, which is the direct force leading to the breaking of the object, as shown in Equation (2):

$$P_s = \frac{1}{2}\rho v^2 \quad (2)$$

where,  $\rho$  is the density of the fluid,  $\text{kg/m}^3$ ,  $v$  is the propagation velocity,  $\text{m/s}$ .

From Equation (2), it can be concluded that the greater the velocity of the fluid, the greater the impact force. In this paper, the maximum velocity in X-axis of the water jet at 100 mm from the end face of the nozzle is taken as index 1 to study three key structural parameters in Section 2.

In addition, through many field experiments, it is found that in the process of coal breaking and punching by water jet, besides the punching depth, the effective punching area is also an important index to measure the water jet performance. The larger the punching area is, the better the effect of gas release is. Given that the numerical model is axisymmetric, data with velocity decay within 15% at 100 mm from the nozzle outlet are selected to calculate the effective extension distance in Y-axis [37], and which is as

index 2. According to the initial structural parameters of the nozzle in Table 2, the model is established.

**Table 2.** Structure parameter of the nozzle.

Structure Parameter	Numerical Value
Contraction angle $\theta$ ( $^{\circ}$ )	30
Length-to-diameter ratio $l/d$	2
Divergence angle $\gamma$ ( $^{\circ}$ )	0

According to the above setting conditions, the velocity vector diagrams of the water jet at different times are calculated numerically by CFD, as shown in Figure 5.

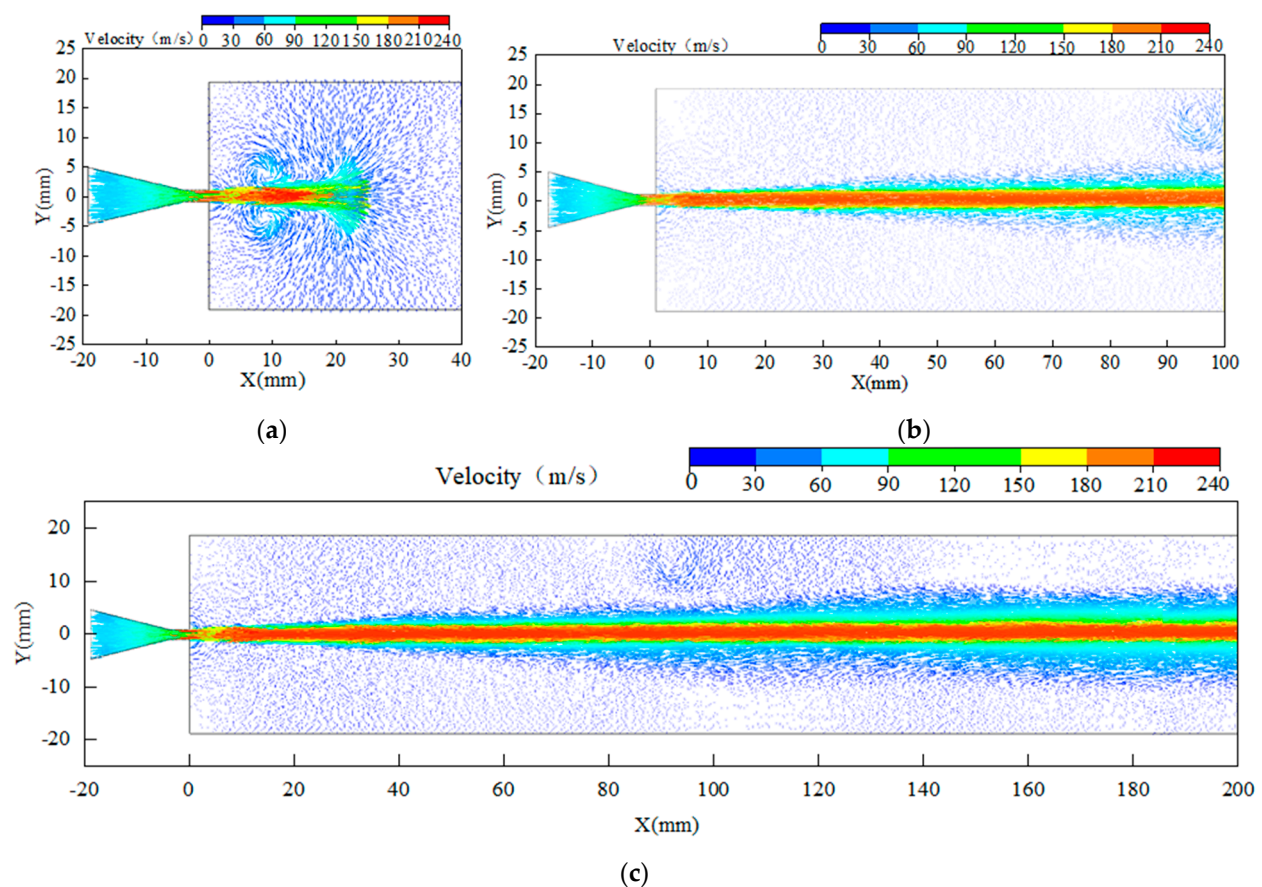


**Figure 5.** Velocity vector of the water jet at different times: (a)  $t = 0.02$  ms; (b)  $t = 0.8$  ms; (c)  $t = 2$  ms.

It can be seen from Figure 5 that the velocity of the water jet increases sharply after the contraction angle, but the contraction angle is too large will intensify the collision between the water jet and the wall, resulting in local turbulence effect, which will increase the velocity loss of the water jet. The existence of the cylindrical section will stabilize the flow and reduce the local turbulence effect of the water jet. However, when the cylindrical section is long, the flow resistance will increase and reduce the outlet velocity. When there is divergence angle in the nozzle, a convergent-divergent nozzle will be formed, which will produce a certain cavitation effect and significantly improve the outlet velocity. In addition, the existence of divergence angle will also reduce the wall adhesion effect and further improve the outlet velocity of the water jet.

When the high-speed water jet is sprayed into the air, due to the large velocity difference, there is a surface of discontinuity between the two fluids and the surface of discontinuity is unstable. Once disturbed, it will fluctuate and form a vortex, which

will strongly suck the surrounding air, forming a high-speed water-air mixture. With the development of turbulence, more and more air is sucked and moving together with the water jet, and the jet boundary is also gradually expanded to both sides to expand the effective strike area of the water jet. However, at the same time, the violent energy exchange will also reduce the maximum velocity in X-axis. The maximum velocity in X-axis is 199.86 m/s, and the effective extension distance in Y-axis is 2.424 mm with the initial design structural parameters of the nozzle. In order to further improve these two target values, the key structural parameters of the nozzle need to be optimized.

### 3. Multi-Objective Collaborative Optimization Design and Analysis

When considering the influence of multiple key structural parameters on multiple indexes at the same time, it is difficult to reveal the complex coupling relationship between multiple parameters and multiple indexes of the nozzle only by the numerical simulation method. Therefore, based on the numerical simulation, the orthogonal test method is used to explore the influence law of key structural parameters on the maximum velocity in X-axis and the effective extension distance in Y-axis, find out the primary and secondary order of the influence of each factor, and get the preliminary optimization parameters. Then, a back propagation (BP) neural network algorithm and genetic algorithm (GA) are complemented each other to establish a balanced and accurate collaborative optimization scheme, calculate the optimal design parameters of the nozzle, and predict the target value [38].

#### 3.1. Collaborative Optimization Scheme Design

BP neural network is a feed-forward neural network trained according to the error back propagation algorithm by simulating the network of human brain neurons. BP neural network is composed of input layer, hidden layer and output layer, and each layer contains a certain number of neurons, which are usually determined according to the input parameters, output parameters and empirical equations. GA is an optimization algorithm based on the survival of the fittest principle, which realizes highly parallel and adaptive global search in parameter space through selection, crossover and mutation. However, GA is easy to fall into the local optimal solution in the calculation process. To overcome this drawback, BP neural network and GA are combined, and the powerful nonlinear mapping ability of BP neural network is used to calculate the individual fitness of the population in GA. Then, GA is used for population optimization to find the individual with the optimal fitness (i.e., the optimal design parameters) [39–43]. The collaborative optimization design scheme is shown in Figure 6.

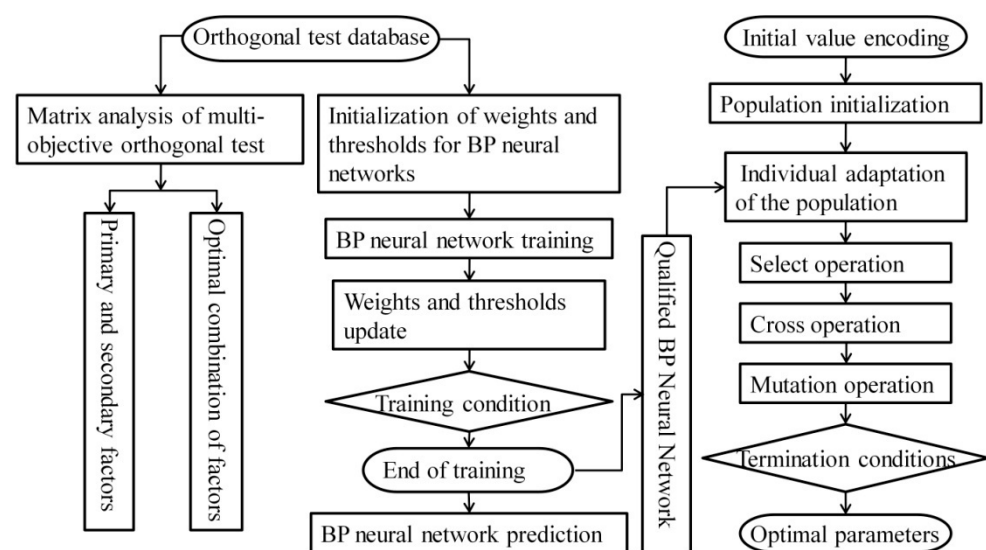


Figure 6. Scheme flow of concurrent design for multi-variable multi-objective.

### 3.1.1. Multi–Objective Orthogonal Test Matrix

According to the results of previous research and field experimental requirements, the value range of the three key parameters selected is shown in Table 3, and three levels of each key parameter are selected. The maximum velocity in X-axis and effective extension distance in Y-axis of the water jet at 100 mm away from the nozzle outlet are selected as inspection indexes. Given that the model is axisymmetric, the effective extension distance in Y-axis is replaced by a half-value. CFD is used for simulation calculation to establish the full factor orthogonal test table, as shown in Table 4, which provides more samples for neural network training. According to the range of the value in Table 3, the contraction angle  $\theta$  is taken as  $30^\circ$ ,  $50^\circ$ , and  $70^\circ$ , respectively, the length-to-diameter ratio  $l/d$  is taken as 2, 2.5, and 3, respectively, and the divergence angle  $\gamma$  is taken as  $0^\circ$ ,  $10^\circ$ , and  $15^\circ$ , respectively, to construct the nozzle model. CFD is used for simulation calculation to establish the full factor orthogonal test table, as shown in Table 4 (which provides more samples for neural network training).

**Table 3.** Initial value and value range of key parameters.

Parameter	Initial Value	Range of the Value
A ( $\theta$ )	$30^\circ$	$30\text{--}70^\circ$
B ( $l/d$ )	2	2–3
C ( $\gamma$ )	$0^\circ$	$0\text{--}15^\circ$

**Table 4.** Orthogonal test database.

Factors	A	B	C	Maximum Velocity in X-axis (m/s)	Effective Extension Distance in Y-axis (mm)
Test Number	1( $^\circ$ )	2	3( $^\circ$ )		
1	30	2	0	199.865	1.212
2	30	2	10	199.868	1.323
3	30	2	15	198.397	1.463
4	30	2.5	0	200.393	1.303
5	30	2.5	10	199.424	1.503
6	30	2.5	15	198.118	1.563
7	30	3	0	199.879	1.221
8	30	3	10	200.024	1.402
9	30	3	15	198.35	1.532
10	50	2	0	200.484	1.242
11	50	2	10	199.181	1.341
12	50	2	15	197.16	1.502
13	50	2.5	0	199.382	1.283
14	50	2.5	10	198.277	1.522
15	50	2.5	15	198.476	1.582
16	50	3	0	199.426	1.281
17	50	3	10	198.39	1.401
18	50	3	15	195.748	1.441
19	70	2	0	198.331	1.183
20	70	2	10	195.775	1.361
21	70	2	15	188.234	1.421
22	70	2.5	0	198.936	1.191
23	70	2.5	10	195.603	1.381
24	70	2.5	15	193.189	1.602
25	70	3	0	199.225	1.101
26	70	3	10	195.284	1.321
27	70	3	15	191.606	1.522

### 3.1.2. Analysis of Multi–Objective Orthogonal Test Matrix

There are many methods to deal with multi-objective optimization problems. At present, the simplest and most effective one is to coordinate and compromise each index,

make each index at the optimal level as much as possible, and finally select the optimal compromise solution for multiple objectives that meet the constraints at the same time. In order to ensure the multi-objective optimization effect, according to the data obtained from the orthogonal test, the matrix of the water jet target layer, factor layer and horizontal layer under multi-objective is established, and the weight of each factor is accurately determined by weight analysis method. The matrix analysis model is shown in Table 5.

**Table 5.** Matrix analysis model of multi-objective orthogonal test.

Hierarchical Structure	Model
Target layer	The two indexes
Factor layer	A, B, C
Horizontal layer	A <sub>1</sub> –A <sub>3</sub> , B <sub>1</sub> –B <sub>3</sub> , C <sub>1</sub> –C <sub>3</sub>

$K_{ij}$  is the arithmetic mean of the results obtained at the  $j$ -th level of factor  $i$ . Both target expectations are as high as possible, so that the target layer matrix is  $M = \{M_v, M_y\}$ , where,  $M_v$  is the target matrix of the maximum velocity in X-axis and  $M_y$  is the target matrix of the effective extension distance in Y-axis, the target layer matrix is as follows:

$$M = \begin{pmatrix} k_{11} & 0 & 0 \\ k_{12} & 0 & 0 \\ k_{13} & 0 & 0 \\ 0 & k_{21} & 0 \\ 0 & k_{22} & 0 \\ 0 & k_{23} & 0 \\ 0 & 0 & k_{31} \\ 0 & 0 & k_{32} \\ 0 & 0 & k_{33} \end{pmatrix} \quad (3)$$

Let  $T_i = 1 / \sum_{j=1}^3 k_{ij}$ , where  $\sum_{j=1}^3 k_{ij}$  denotes the sum of the arithmetic means of the results obtained at each level of factor  $i$ , the factor layer matrix is defined as  $T = \{T_v, T_y\}$ , where  $T_v, T_y$  are the factor layer matrices of the maximum velocity in X-axis and the effective extension distance in Y-axis, respectively, and the factor layer matrix is as follows.

$$T = \begin{pmatrix} T_1 & 0 & 0 \\ 0 & T_2 & 0 \\ 0 & 0 & T_3 \end{pmatrix} \quad (4)$$

Let  $S_i = R_i / \sum_{i=1}^3 R_i$ , where 7 denotes the range of the factor  $i$ -th in the orthogonal test, the horizontal layer matrix is defined  $S = \{S_v, S_y\}$ , where,  $S_v, S_y$  are the horizontal layer matrices of the maximum velocity in X-axis and the effective extension distance in Y-axis, respectively, and the horizontal layer matrix is as follows.

$$S = (S_1 \ S_2 \ S_3)^T \quad (5)$$

The key analysis of multi-objective orthogonal test matrix is to determine the weight of each objective. The weight is directly related to the accuracy and reliability of the results of each factor in the global optimization. Therefore, the total weight matrix of the target value is defined as follows:

$$w = MTS = (w_{A1}, w_{A2}, w_{A3}, \dots, w_{C1}, w_{C2}, w_{C3})^T \quad (6)$$

where, 1 denotes the weight value of the influence of the  $j$ -th level of factor  $A$  on this target, which can not only reflect the influence degree of this level on the target, but also can be used as the range value of factor  $A$ .

$w_v$  is the weight matrix of the maximum velocity in X-axis,  $w_y$  is the weight matrix of the effective extension distance in Y-axis, and  $w$  is the total weight matrix of multiple targets. The equations are as follows:

$$\begin{aligned}w_v &= M_v T_v S_v \quad w_y = M_y T_y S_y \\w &= (w_v + w_y) / 2\end{aligned}\quad (7)$$

The data in Table 4 are calculated according to Equations (3)–(7), and the total weight matrix for each level of the different factors is obtained, as shown in Table 6.

**Table 6.** Value of total weight matrix for multi-objective evaluation.

Weight Matrix	Numerical Value	Weight Matrix	Numerical Value	Weight Matrix	Numerical Value
$W_{A1}$	0.093052	$W_{B1}$	0.062866	$W_{C1}$	0.165514
$W_{A2}$	0.093238	$W_{B2}$	0.065545	$W_{C2}$	0.17845
$W_{A3}$	0.090959	$W_{B3}$	0.063391	$W_{C3}$	0.186986

By analyzing the weight matrix in Table 6, it can be concluded that the maximum total weight of the three levels of each factor is  $A_2 = 0.093238$ ,  $B_2 = 0.065545$ , and  $C_3 = 0.186986$ , respectively. Therefore, the optimal combination of factors under multi-objective key structural parameters of the nozzle is  $A_2B_2C_3$ . The specific parameters are the contraction angle  $\theta = 50^\circ$ , the length-to-diameter ratio  $l/d = 2.5$  and the divergence angle  $\gamma = 15^\circ$ . This combination is the 15th group in Table 4, at which the maximum velocity in X-axis is  $v = 198.476$  m/s and the effective extension distance in Y-axis is  $y = 3.164$  mm. The analysis of the data in Table 4 shows that there is no other combination of the nozzle parameters whose two target values are greater than this combination. Therefore, from the perspective of multi-objective optimization, the combination  $A_2B_2C_3$  is the optimal combination in the full factor orthogonal test table, which also proves the accuracy of the weight matrix analysis. The matrix analysis results of multi-objective orthogonal test are shown in Table 7.

**Table 7.** Results of multi-objective orthogonal test matrix analysis.

Category	Result		
Sensitivity of each factor	A 0.2772	B 0.1918	C 0.5310
Primary and secondary order of factors	C > A > B		
Optimal combination	$A_2B_2C_3$		

### 3.2. Multi-Objective Collaborative Optimization

Although the orthogonal test is representative and efficient, it is difficult to ensure that the result is the optimal value in the whole interval since the value of each factor is fixed-point discrete value, and only three levels are taken for each factor in this paper. Therefore, the multi-parameter and multi-objective collaborative optimization method combining BP neural network and GA is adopted, and the data in the orthogonal test are used as the training library to obtain the relationship model between multi-parameters and multi-objective. The seamless and accurate optimization is realized in the parameter interval, and the optimal value in the whole interval is obtained.

### 3.2.1. Network Training

In order to ensure the stability and accuracy of BP neural network training, the data are expanded on the basis of the original 27 groups of orthogonal test data. According to influence primary and secondary order of factors in Table 7, the contraction angle and divergence angle are selected. The contraction angle of 30° and 50° are replaced by 40° and 60° in the range of values of each parameter in Table 3 for numerical simulation calculation, and 18 new groups of data are obtained. Then, the divergence angle of 0° is replaced by the original 5° for numerical simulation calculation. A total of 9 new groups of data are obtained again, and these 54 groups of data are used as the sample training database of BP neural network.

The BP neural network consists of three layers: an input layer, hidden layer, and output layer. The neurons of input and output layer correspond to the key structural parameters of the nozzle and the optimization objectives, respectively. The hidden layer is the link connecting the input layer and the output layer, and its main function is to learn the nonlinear laws contained in the data through continuous training [44–46]. The hidden layer can be either multi-layer or single-layer structure. The universal approximation theorem shows that as long as the number of neurons in the hidden layer is selected appropriately, the BP neural network with one hidden layer can approach any multivariable function. Therefore, the hidden layer of the neural network established in this paper is set as one layer, and the design equation for the number of neurons in the hidden layer is as follows:

$$\sqrt{m+n} + 1 \leq k \leq \sqrt{m+n} + 10 \quad (8)$$

In the above equation, the number of neurons in the input layer  $m = 3$ , the number of neurons in the output layer  $n = 2$ ,  $K$  is the number of neurons in the hidden layer, and its value range is 3–12.

According to the study, the tansig–purelin transfer function is used between the three-layers of the network, the selection of network training function is shown in Table 8, the training rate is set to 0.01, the training times is 500, and the expected error is  $1 \times 10^{-5}$ .

**Table 8.** Selection of training function.

Serial Number of the Function	Training Function	Training Times	Serial Number of the Function	Training Function	Training Times
1	Traingda	115 times to reach the target	5	Traincgf	22 times to reach the target
2	Trainbfg	29 times to reach the target	6	Trainscg	26 times to reach the target
3	Trainoss	20 times to reach the target	7	Trainrp	76 times to reach the target
4	Traincgb	17 times to reach the target	8	Trainlm	19 times to reach the target

The change of mean square error with the number of neurons in the hidden layer and training function is shown in Figure 7. It can be seen that when the training functions are different, in order to minimize the mean square deviation, the hidden layer needs to select different numbers of neurons. Overall, the mean square error of training functions No. 2 and No. 4 is small, and the mean square error of training functions No. 1 and No. 5 is large.

When the optimal number of neurons in the hidden layer is determined for all eight training functions, the database is trained, respectively. The test set correlation coefficient of each training function is shown in Figure 8. It can be seen that the test set correlation coefficient obtained by training function No. 8 is the highest. Based on the results in Figures 7 and 8 and Table 8, it is finally determined that the training function is trainlm and the optimal number of neurons in the hidden layer is 5.

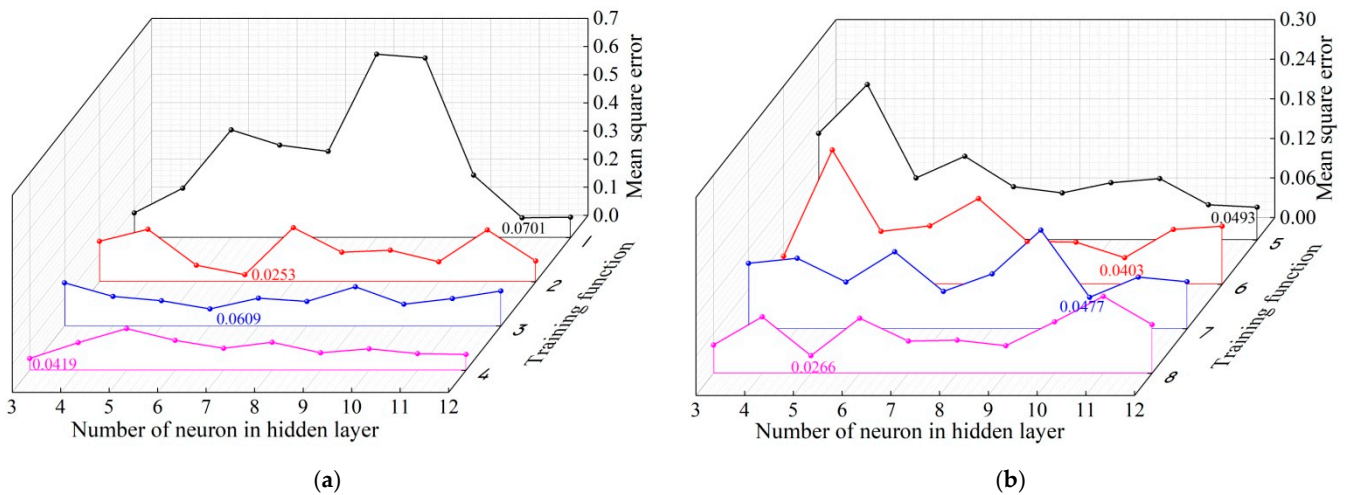


**Figure 7.** Change of mean square error of different training functions with the number of neurons in the hidden layer: (a) training functions No. 1 to No. 4; (b) training functions No. 5 to No. 8.

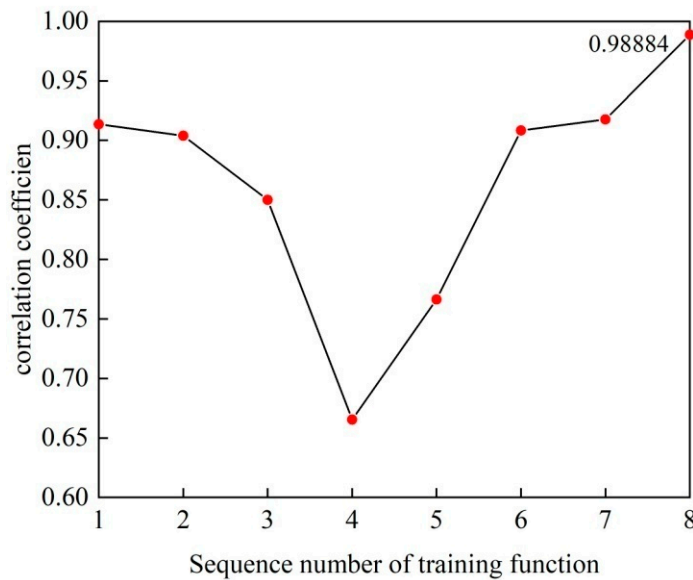


**Figure 8.** Correlation coefficients of different training function.

### 3.2.2. Training Network Analysis and Verification

The BP neural network obtained is trained by the orthogonal test database, the sample data matching results are shown in Figure 9. It can be seen that the fit between the predicted and actual output of the trained network model is as high as 98.88%, which has a very good fitting effect.

To further verify the reliability of the obtained network, data No. 1, No. 5, No. 10, No. 15, and No. 20 from the orthogonal test library are randomly selected for testing, and the comparison between the actual values of the test samples and the predicted values of the network is shown in Figure 10 and Table 9. It can be seen from Table 9 that the relative error is controlled within 5%, which meets the accuracy requirements in engineering practice and indicates that the model achieves a high degree of network recognition.

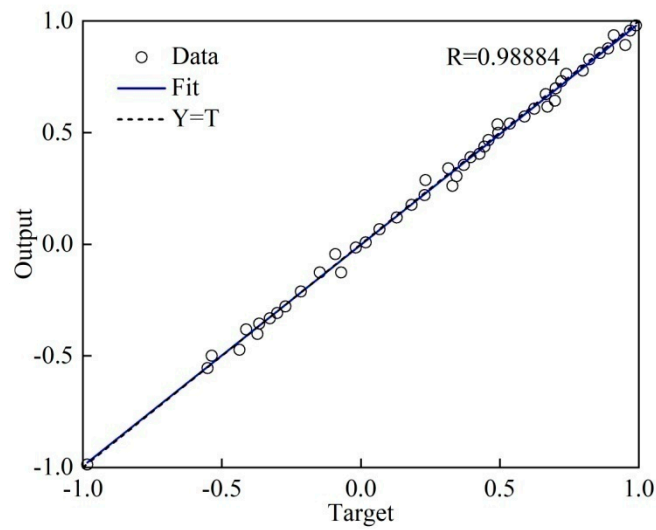


Figure 9. Fitness curve of sample.

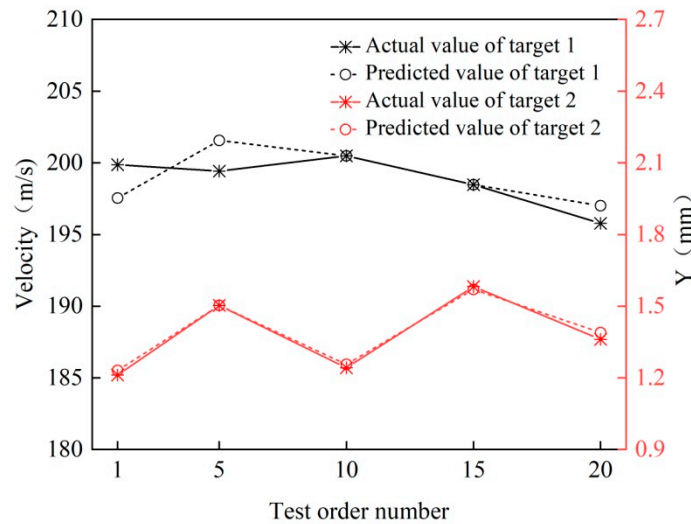


Figure 10. Error analysis between actual value and prediction value.

Table 9. Error between actual value and predicted value of BP neural network.

Evaluation Index	Category	Test 1	Test 2	Test 3	Test 4	Test 5
Target 1	Actual value (m/s)	199.865	199.424	200.484	198.476	195.775
	Predicted value (m/s)	197.541	201.56	200.484	198.476	197.003
	Relative error (m/s)	1.16	1.07	0	0	0.63
Target 2	Actual value (m/s)	1.212	1.503	1.242	1.582	1.361
	Predicted value (m/s)	1.231	1.503	1.256	1.57	1.389
	Relative error (%)	1.57	0	1.13	0.76	2.05

### 3.2.3. Optimal Parameter Determination

The core of GA is fitness function calculation, selection, crossover, and mutation operation. The value range of each key optimization parameter in Table 3 is used as the optimization interval for the parameters of the GA. The BP neural network trained in the previous section is used to calculate the individual fitness of the population in the GA. The selection strategy based on the fitness ratio (i.e., the roulette wheel method) is used in the selection operation. The real number crossover method is used in the crossover operation, and the random method is used in the variation operation to select the variant genes. After

program debugging, the maximum evolutionary algebra is 50, the crossover probability is 0.4 and the mutation probability is 0.2 in this paper.

The GA is used to search and optimize the key parameters of the nozzle in a global range, and the optimization process is shown in Figure 11. With the generation by generation evolution of the genetic algorithm, the optimization goal approaches the optimal solution. After 30 generations, the target value search process is basically completed, and the results of the multi-parameter and multi-objective optimization are shown in Table 10.

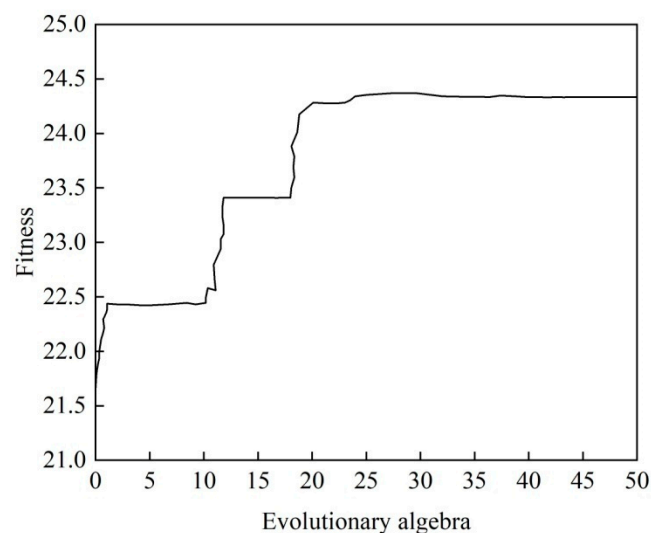


Figure 11. The process of optimization.

Table 10. Comparison of results before and after collaborative optimization.

Category	Optimization Parameter			Category	Optimization Parameter		
	Contraction Angle $\theta$ ( $^{\circ}$ )	Length-to-Diameter Ratio $l/d$	Divergence Angle $\gamma$ ( $^{\circ}$ )		Contraction Angle $\theta$ ( $^{\circ}$ )	Length-to-Diameter Ratio $l/d$	Divergence Angle $\gamma$ ( $^{\circ}$ )
Initial value	30	2	0	Optimal value of orthogonal test	50	2.5	15
Collaborative optimization value	42.512	2.5608	12.431	Collaborative optimization value	42.512	2.5608	12.431
Change rate	41.71%	28.04%	$\infty$	Change rate	14.98%	2.43%	-17.13%
Category	Optimization Target		Category	Optimization Target			
	Target 1 (m/s)	Target 2 (mm)		Target 1 (m/s)	Target 2 (mm)		
Initial value	199.865	1.212	Optimal value of orthogonal test	198.476	1.582		
Collaborative optimization value	203.77	1.632	Collaborative optimization value	203.77	1.632		
Optimization rate	1.95%	34.65%	Optimization rate	2.67%	3.16%		

It can be seen from the data in Table 10 that after the multi-parameter and multi-objective collaborative optimization, the three key parameters of the nozzle have changed significantly compared with the initial values and the optimal combination of parameters in the orthogonal test scheme, the maximum velocity in X-axis and effective extension distance in Y-axis have been greatly improved, and the two objectives have been better optimized in the desired direction. The combination of parameters optimized by the intelligent algorithm is not the optimal parameters in the orthogonal test scheme, which again proves that the combination of BP neural network and GA can be used to achieve seamless interval optimization search.

## 4. Coal Breaking and Punching Experiment

### 4.1. Experiment Scheme

Nozzle No. 2 is made according to the optimal value of orthogonal test, and nozzle No. 3 is made according to the structural optimal parameters obtained from multi-parameter and multi-objective collaborative optimization, which is verified by briquette erosion experiment together with the original nozzle No. 1, and they are verified together with the initial nozzle No. 1 for the coal breaking and punching experiment. The schematic diagram of the experimental equipment is shown in Figure 12. A relief valve is used to regulate the pressure of the system to ensure that the inlet pressure of the water jet is stabilized at 20 MPa. The high-pressure turbine flowmeter with electronic display is used to detect the water flow of each experiment. The field experimental equipment is shown in Figure 13.

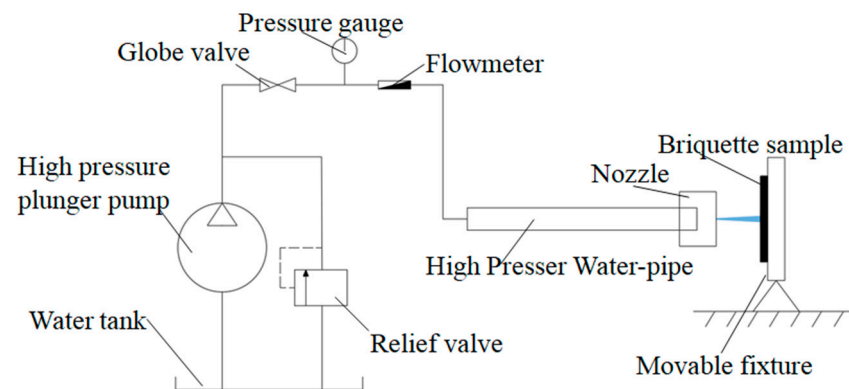


Figure 12. Schematic diagram of equipment.

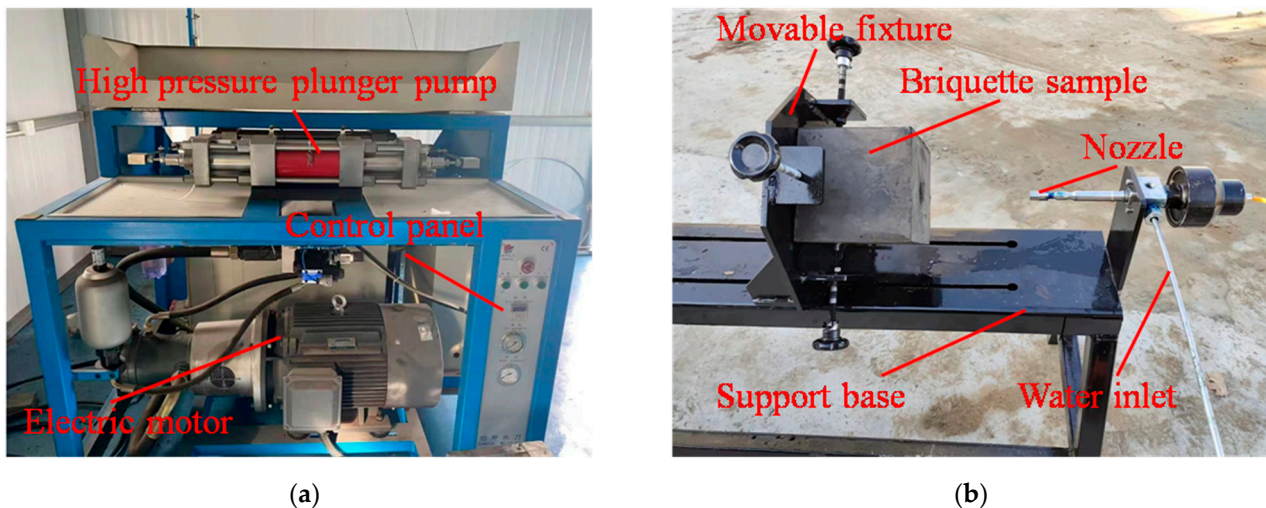


Figure 13. Experiment equipment: (a) pumping station; (b) equipment of the water jet.

### 4.2. Preparation of Briquette

The briquette specimens selected for this experiment are self-made in the mineral Safety Laboratory of North China University of Science and Technology. Coal-dust is used as the main raw material, together with a certain proportion of cement, gypsum and sodium humate to make the specimens with compressive strength of 15 MPa and side length of 150 mm. In order to ensure the complete hardness increase of the briquette specimens, they are maintained in the exact same environment for 28 days. When the maintenance period is over, five specimens are randomly selected for compressive strength testing. The test results are shown in Table 11.

**Table 11.** Test results of compressive strength of coal type.

Specimen Number	1	2	3	4	5
Compressive strength/MPa	14.9	15.1	15.0	15.0	14.8
Absolute error of compressive strength	0.67%	0.67%	0	0	1.33%

It can be seen from the data in Table 11 that the compressive strength of the five randomly selected test specimens is not exactly the same, which may be caused by the proportion error of each raw material during the fabrication of the specimens, but the absolute error of compressive strength of these five specimens is within 2%, which meets the requirements of engineering experiments and can be used for erosion experiments.

#### 4.3. Experiment Analysis

Before the experiment, the briquette specimen is fixed on the support base by the movable fixture, and the distance between the briquette specimen and the nozzle outlet is adjusted to 10 cm. Each punching time is 300 s. Each punching time is 300 s, and the distance between the specimen and the nozzle will be measured and adjusted again after each punching is completed to ensure that the target distance of all of the punching experiments is 10 cm. In order to improve the accuracy of the experiment, each nozzle will carry out three punching experiments, the punching diameter and punching depth to take the arithmetic average of the three experiments for comparison. The effect of punching is shown in Figure 14, and the data are shown in Tables 12 and 13.

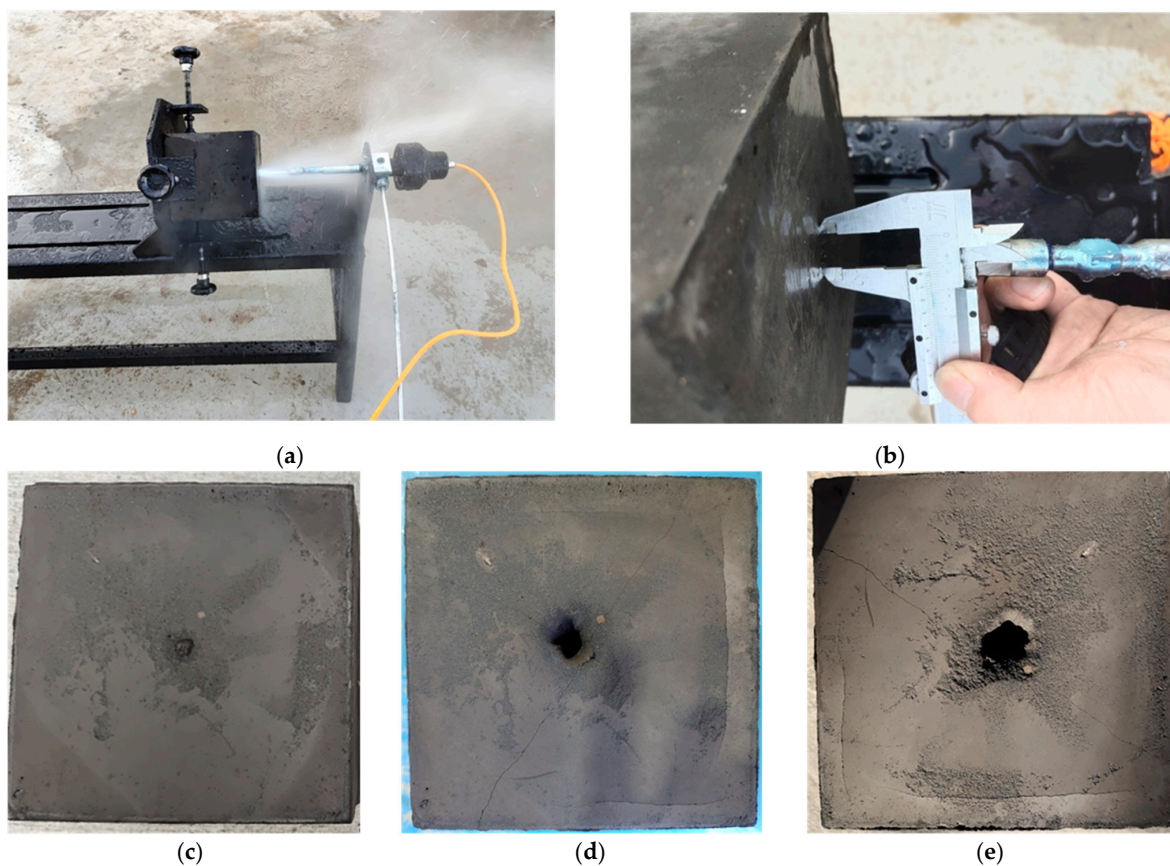


**Figure 14.** Experiment of punching: (a) the punching process; (b) measurement of results; (c) punching effect of the nozzle 1; (d) punching effect of the nozzle 2; (e) punching effect of the nozzle 3.

**Table 12.** Depth of punching.

Nozzle Model	Experiment Number			Arithmetic Mean	Standard Deviation	Improve Rate
	1	2	3			
1	43.3 mm	44.5 mm	44.3 mm	44.03 mm	0.5249	72.71%
2	57.4 mm	57.0 mm	57.7 mm	57.36 mm	0.2867	31.88%
3	75.2 mm	76.4 mm	75.6 mm	75.73 mm	0.4989	optimal value

**Table 13.** Diameter of punching.

Nozzle Model	Experiment Number			Arithmetic Mean	Standard Deviation	Improve Rate
	1	2	3			
1	6.5 mm	6.4 mm	6.3 mm	6.40 mm	0.0816	106.72%
2	10.4 mm	10.7 mm	10.6 mm	10.56 mm	0.1249	25.28%
3	13.2 mm	13.4 mm	13.1 mm	13.23 mm	0.1248	optimal value

It can be seen from the data in Table 12 that although the measured punching depth after each experiment of the three nozzles is not exactly the same, all of the data are within two standard deviation intervals, which is compliant with engineering standards, and the experimental data are stable and reliable. The same is true for the data in Table 13. The measured diameter of each nozzle after punching fluctuates little and is within two standard deviation intervals.

By comparing the data in Tables 12 and 13, it can be seen that the punching effect of the nozzle 3 is the best, in terms of punching depth, which is 72.71% higher than nozzle 1, 31.88% higher than nozzle 2, and in terms of punching diameter, which is 106.72% and 25.28% higher, respectively. This is consistent with the trend in the collaborative optimization analysis in Section 3.2, indicating that the water jet performance of the nozzle has been effectively improved through the intelligent collaborative optimization scheme. Comparing the results of the nozzle 2 and nozzle 1, it can be seen that nozzle 2 is better than nozzle 1 in punching depth and diameter, and the punching depth and diameter are increased by 30.27% and 65.00%, respectively. Combined with the analysis in Section 3.2 of the multi-objective weight, it can be seen that the optimization target 1 (the maximum velocity in the X-axis) and optimization target 2 (the effective extension distance in the Y-axis) affect each other. When the two target values are considered together, the coal breaking and punching effect will be better, which also proves the correctness of multi-objective weight analysis and lays a reliable foundation for subsequent collaborative optimization.

## 5. Conclusions

In this study, a multi-parameter and multi-objective optimization method is proposed to optimize the coal breaking and punching nozzle, and the best combination of parameters for the nozzle is obtained. After experimental verification, the water jet performance of the optimized nozzle is improved. The specific research results are as follows:

- (1) The multi-objective weight analysis method is used to optimize the parameters of the high-pressure water jet coal breaking and punching nozzle. It is concluded that the primary and secondary order affecting the maximum velocity in X-axis and effective extension distance in Y-axis of the water jet is as follows: divergence angle, contraction angle and length-to-diameter ratio. For the multi-index model, the weight analysis method can efficiently and accurately analyze the influence of parameters on multiple indexes.
- (2) The multi-objective collaborative optimization of the nozzle is carried out by using the collaborative optimization scheme of the BP neural network and GA. It is concluded that the optimal combination of its structure is as follows: the contraction angle is  $\theta = 42.512^\circ$ , the length-to-diameter ratio is  $l/d = 2.5608$ , and the divergence angle is  $\gamma = 12.431^\circ$ . Compared with the nozzle before optimization, the punching

depth is increased by 72.71% and the punching diameter is increased by 106.72%. The combination of BP neural network and GA not only improves the global search efficiency, but also avoids falling into the local optimal solution.

- (3) The water jet punching experiment shows that the punching depth and punching diameter affect each other. When multiple objectives are considered synergistically, the performance of the water jet is significantly improved compared with considering each optimization objective separately, which not only provides a new idea for the optimization of the nozzle structure, but also can be used in other multi-objective and multi-parameter models.

**Author Contributions:** Conceptualization, L.C.; methodology, L.C.; software, M.C.; validation, L.G.; formal analysis, Y.C.; writing—original draft preparation, L.C. and M.C.; writing—review and editing, L.C. and D.G.; supervision, L.C. and D.G.; funding acquisition, L.G. All authors have read and agreed to the published version of the manuscript.

**Funding:** This research was funded by the National Natural Science Foundation of China, grant number 51874012, and this research was funded by the North China Institute of Aerospace Engineering, grant number KY202104.

**Institutional Review Board Statement:** Not applicable.

**Informed Consent Statement:** Not applicable.

**Data Availability Statement:** Not applicable.

**Conflicts of Interest:** The authors declare no conflict of interest.

## References

- Shen, Z.H. *Water Jet Theory and Technology*; China University of Petroleum Press: Dongying, China, 1998.
- Liu, X.; Liu, S.; Ji, H. Mechanism of rock breaking by pick assisted with water jet of different modes. *J. Mech. Sci. Technol.* **2015**, *29*, 5359–5368. [[CrossRef](#)]
- Fuse, K.; Chaudhari, R.; Vora, J.; Patel, V.K.; de Lacalle, L.N.L. Multi-Response Optimization of Abrasive Waterjet Machining of Ti6Al4V Using Integrated Approach of Utilized Heat Transfer Search Algorithm and RSM. *Materials* **2021**, *14*, 7746. [[CrossRef](#)] [[PubMed](#)]
- Han, W.; Zhou, G.; Gao, D.; Zhang, Z.; Wei, Z.; Wang, H.; Yang, H. Experimental analysis of the pore structure and fractal characteristics of different metamorphic coal based on mercury intrusion-nitrogen adsorption porosimetry. *Powder Technol.* **2020**, *362*, 386–398. [[CrossRef](#)]
- Sharma, V.; Chattopadhyaya, S.; Hloch, S. Multi response optimization of process parameters based on Taguchi—fuzzy model for coal cutting by water jet technology. *Int. J. Adv. Manuf. Technol.* **2011**, *56*, 1019–1025. [[CrossRef](#)]
- Liu, Y.; Zhang, T.; Liu, X. Analysis of the stress wave effect during coal breakage by a high-pressure abrasive air jet. *Adv. Mech. Eng.* **2018**, *10*, 1687814018782302. [[CrossRef](#)]
- Liu, C.; Xia, B.; Lu, Y. Coal bed methane extraction using the self-oscillating water jet slotting method. *Energies* **2018**, *11*, 897. [[CrossRef](#)]
- Zhang, X.Z.; Wiśniewski, P.; Dykas, S.; Zhang, G. Permeability Enhancement Properties of High-Pressure Abrasive Water Jet Flushing and Its Application in a Soft Coal Seam. *Front. Energy Res.* **2021**, *9*, 679623. [[CrossRef](#)]
- Wen, J.W.; Chen, C. Optimizing the Structure of the Straight Cone Nozzle and the Parameters of Borehole Hydraulic Mining for Huadian Oil Shale Based on Experimental Research. *Energies* **2017**, *10*, 2021. [[CrossRef](#)]
- Chen, J.; Guo, L.W.; Hu, Y.W.; Chen, Y. Internal structure of a jet nozzle for coal bed methane mining based on airfoil curves. *Shock Vib.* **2018**, *2018 Pt 11*, 3840834. [[CrossRef](#)]
- Li, H.S.; Liu, S.Y.; Jia, J.G.; Wang, F.C.; Guo, C.W. Numerical simulation of rock-breaking under the impact load of self-excited oscillating pulsed water jet. *Tunn. Undergr. Sp. Technol.* **2020**, *96*, 179–192. [[CrossRef](#)]
- Liu, Y.; Cui, J.W.; Jian, P.; Liu, X.T. Effect of the nozzle structure on coal breakage of SC-CO<sub>2</sub> used for well drilling. *Geomech. Geophys. Geo-Energy Geo-Resour.* **2020**, *6*, 46–67. [[CrossRef](#)]
- Hong, C.Y.; Yang, R.Y.; Huang, Z.W.; Liu, W.; Chen, J.X.; Cong, R.C. Experimental investigation on coal-breakage performances by abrasive nitrogen-gas jet with a conical nozzle. *Int. J. Rock Mech. Min.* **2021**, *142*, 104781. [[CrossRef](#)]
- Wen, J.W.; Chen, C.; Qi, Z.W.; Campos, U.; Pei, X.J. Bionic optimum design of straight cone nozzle and the effectiveness evaluation of reducing fluid resistance. *J. Braz. Soc. Mech. Sci.* **2019**, *41*, 358–369. [[CrossRef](#)]
- Wen, J.W.; Qi, Z.W.; Behbahani, S.S.; Pei, X.J.; Iseley, T. Research on the structures and hydraulic performances of the typical direct jet nozzles for water jet technology. *J. Braz. Soc. Mech. Sci.* **2019**, *41*, 570–585. [[CrossRef](#)]

16. Zhang, C.; Wen, P.; Yuan, Y.; Fan, X.J. Evaluation and optimal design of supersonic nozzle for laser-assisted oxygen cutting of thick steel sections. *Int. J. Adv. Manuf. Technol.* **2016**, *86*, 1243–1251. [[CrossRef](#)]
17. Chen, L.H.; Cheng, M.Z.; Cai, Y.; Guo, L.W.; Gao, D.R. Design and Optimization of High-Pressure Water Jet for Coal Breaking and Punching Nozzle Considering Structural Parameter Interaction. *Machines* **2022**, *10*, 60. [[CrossRef](#)]
18. Juraeva, M.; Song, D.J.; Kang, D.J. Computational optimization approach to design a water-jet nozzle for a water-jet loom using the design of experiment method. *J. Mech. Sci. Technol.* **2019**, *33*, 631–637. [[CrossRef](#)]
19. Hira, O.; Yücedağ, S.; Samankan, S. Numerical and experimental analysis of optimal nozzle dimensions for FDM printers. *Prog. Addit. Manuf.* **2022**, *1*, 1–14. [[CrossRef](#)]
20. Wang, A.; Sun, P.F.; Zhang, Z.W.; He, B.M.; Meng, G.Y.; Yang, J.; Cheng, X.H. Numerical Simulation and Experimental Study on High-Pressure Water Jet Descaling in Coal Mine Drainage Pipeline. *Iran. J. Sci. Technol. Trans. Mech. Eng.* **2022**, *46*, 113–130. [[CrossRef](#)]
21. Tang, S.N.; Zhu, Y.; Yuan, S.Q. Intelligent Fault Diagnosis of Hydraulic Piston Pump Based on Deep Learning and Bayesian Optimization. *ISA Trans.* **2022**, *1*, 1–16. [[CrossRef](#)]
22. Tang, S.N.; Zhu, Y.; Yuan, S.Q. A Novel Adaptive Convolutional Neural Network for Fault Diagnosis of Hydraulic Piston Pump with Acoustic Images. *Adv. Eng. Inform.* **2022**, *52*, 101554. [[CrossRef](#)]
23. Tang, S.N.; Zhu, Y.; Yuan, S.Q. An adaptive deep learning model towards fault diagnosis of hydraulic piston pump using pressure signal. *Eng. Fail. Anal.* **2022**, *138*, 106300. [[CrossRef](#)]
24. Tang, S.N.; Zhu, Y.; Yuan, S.Q. Intelligent Fault Identification of Hydraulic Pump Using Deep Adaptive Normalized CNN and Synchrosqueezed Wavelet Transform. *Reliab. Eng. Syst. Saf.* **2022**, *224*, 108560. [[CrossRef](#)]
25. Ding, Y.; Wang, J.; Jiang, B.; Li, Z.; Xiao, Q.; Wu, L.; Xie, B. Multi-Objective Optimization for the Radial Bending and Twisting Law of Axial Fan Blades. *Processes* **2022**, *10*, 753. [[CrossRef](#)]
26. Cain, E.; Konstantinos, P.; Fatos, X. Utilizing artificial neural networks and genetic algorithms to build an algo-trading model for intra-day foreign exchange speculation. *Math. Comput. Model.* **2013**, *58*, 1249–1266. [[CrossRef](#)]
27. Maa, A.; Oab, B.; Az, C. Parametric analysis and minimization of entropy generation in bioinspired magnetized non-newtonian nanofluid pumping using artificial neural networks and particle swarm optimization—Science Direct. *Therm. Sci. Eng. Prog.* **2021**, *24*, 100930. [[CrossRef](#)]
28. Chen, B.; Gao, D.R.; Li, Y.B. Experimental analysis of spray behavior and lubrication performance under twin-fluid atomization—Science Direct. *J. Manuf. Process.* **2021**, *61*, 561–573. [[CrossRef](#)]
29. Zhang, D.; Wang, H.; Liu, J.; Wang, C.; Ge, J.; Zhu, Y.; Chen, X.; Hu, B. Flow Characteristics of Oblique Submerged Impinging Jet at Various Impinging Heights. *J. Mar. Sci. Eng.* **2022**, *10*, 399. [[CrossRef](#)]
30. Faha, B.; Kai, S.A.; Zc, A. Internal two-phase flow and spray characteristics of outside-in-liquid twin-fluid atomizers. *Appl. Therm. Eng.* **2021**, *187*, 116688. [[CrossRef](#)]
31. Hu, B.; Wang, H.; Liu, J.; Zhu, Y.; Wang, C.; Ge, J.; Zhang, Y. A Numerical Study of a Submerged Water Jet Impinging on a Stationary Wall. *J. Mar. Sci. Eng.* **2022**, *10*, 228. [[CrossRef](#)]
32. Xi, B.; Wang, C.; Xi, W. Experimental investigation on the water hammer characteristic of stalling fluid in eccentric casing-tubing annulus. *Energy* **2022**, *1*, 124113. [[CrossRef](#)]
33. Ge, Z.; Zhong, J.; Zhang, J. Structural Optimization of Slotting Nozzle Used to Improve Coal-Seam Permeability. *Appl. Sci.* **2020**, *10*, 699. [[CrossRef](#)]
34. Lu, Y.Y.; Fei, H.; Liu, X.; Ao, X. On the failure pattern of sandstone impacted by high-velocity water jet. *Int. J. Impact Eng.* **2015**, *76*, 67–74. [[CrossRef](#)]
35. Chen, B.; Lu, Y.J.; Li, W.Y. DPM-LES investigation on flow field dynamic and acoustic characteristics of a twin-fluid nozzle by multi-field coupling method. *Int. J. Heat Mass Transf.* **2022**, *192*, 122927. [[CrossRef](#)]
36. Li, W.; Qian, L.; Song, S. Numerical Study on the Influence of Shaping Air Holes on Atomization Performance in Pneumatic Atomizers. *Coatings* **2019**, *9*, 410. [[CrossRef](#)]
37. Azad, M.; Quinn, W.R.; Groulx, D. Mixing in Turbulent Free Jets Issuing from Isosceles Triangular Orifices with Different Apex Angles. *Exp. Therm. Fluid Sci.* **2012**, *39*, 237–251. [[CrossRef](#)]
38. Tian, W.; Liao, Z.; Zhang, J. An optimization of artificial neural network model for predicting chlorophyll dynamics. *Ecol. Model.* **2017**, *364*, 42–52. [[CrossRef](#)]
39. Chen, L.L.; Chen, J.; Wang, C. Modeling of Moisture Content of Subgrade Materials in High-Speed Railway Using a Deep Learning Method. *Adv. Mater. Sci. Eng.* **2021**, *2021*, 6166489. [[CrossRef](#)]
40. Zhu, Y.; Li, G.P.; Tang, S.N.; Wang, R.; Su, H.; Wang, C. Acoustic Signal-based Fault Detection of Hydraulic Piston Pump using a Particle Swarm Optimization Enhancement CNN. *Appl. Acoust.* **2022**, *192*, 108718. [[CrossRef](#)]
41. Zhu, Y.; Li, G.P.; Wang, R.; Tang, S.N.; Su, H.; Cao, K. Intelligent Fault Diagnosis of Hydraulic Piston Pump Combining Improved LeNet-5 and PSO Hyperparameter Optimization. *Appl. Acoust.* **2021**, *183*, 108336. [[CrossRef](#)]
42. Gao, Q.; Zhu, Y.; Liu, J. Dynamics modelling and control of a novel fuel metering valve actuated by two binary-coded digital valve arrays. *Machines* **2022**, *10*, 55. [[CrossRef](#)]
43. Yuan, X.M.; Wang, W.Q.; Zhu, X. Theory Model of Dynamic Bulk Modulus of Aerated Hydraulic Fluid. *Chin. J. Mech. Eng.-En.* **2022**, *4*, 735. [[CrossRef](#)]

44. Wang, S.; Xiao, B.; Ge, Y. Optimization design of slotted fins based on exergy destruction minimization coupled with optimization algorithm. *Int. J. Therm. Sci.* **2020**, *147*, 106133. [[CrossRef](#)]
45. Gao, Q. Nonlinear Adaptive Control with Asymmetric Pressure Difference Compensation of a Hydraulic Pressure Servo System Using Two High Speed On/Off Valves. *Machines* **2022**, *10*, 66. [[CrossRef](#)]
46. Wu, J.; Cheng, Y.M.; Liu, C. A BP Neural Network Based on Improved PSO for Increasing Current Efficiency of Copper Electrowinning. *J. Electr. Eng. Technol.* **2021**, *16*, 1297–1304. [[CrossRef](#)]